The Influence of B, N and Si Doping on the CH₃ Adsorption on the Diamond Surface Based on DFT Calculations

Liang Wang *, Jiangshan Liu and **Tang Tang**

School of Mechanical Engineering, Tongji University, Shanghai 201804, China
* Correspondence: liangwang@tongji.edu.cn; Tel.: +86-021-6958-5790

Abstract: To better understand the influence mechanism of boron, nitrogen and silicon dopants on the growth of chemical vapor deposition (CVD) diamond film, density functional calculations have been performed to reveal the different impact of the impurities on the CH_3 adsorption on diamond surface. The substituted doping and radical doping of diamond (111) and (100) − 2 × 1 surface are both considered. The calculation results indicate that the CH_3 radicals are hardly adsorbed on nitrogen atoms and thus may cause vacancy in the diamond lattice easily. Boron substituted doping will disfavor the adsorption of CH_3 due to the lacking of valence electron. However, the empty p orbitals of boron atom will help the chemical adsorbing of CH_3 radicals. The substituted silicon doping has little influence on the CH_3 adsorption, as Si atom has the same outer valence electron structure with C atom. In the case of radical doping, the adsorption energy of CH_3 will be reduced due to the steric hindrance between NH_2 or SiH_3 with CH_3. The adsorption energy can be slightly enhanced when BH_2 radical is pre-adsorbed on diamond (111) surface. However, the BH_2 pre-adsorbed on diamond (100) − 2 × 1 surface may interact with surface radical carbon site and result in a large reduction of CH_3 adsorption energy. Thus, the boron doping may hinder the formation of the (100) facet during the CVD diamond deposition under a certain condition.

Keywords: boron; silicon; nitrogen; growth mechanism; diamond film; first principles

1. Introduction

Chemical vapor deposition (CVD) diamond films have been wildly used in electronic, mechanical, optical, and various other fields due to their unique properties. Furthermore, CVD is a suitable method to change the properties of diamond films easily [1–5]. Doping the diamond with boron, silicon, nitrogen, phosphorus, lithium or europium allows the semiconductor [6] to form luminescent centers [3,7] or a nitrogen-vacancy (NV) center [8,9]. Additionally, experimental investigations reported that the introduction of impurities into the plasma can also affect the growth rate [10], surface morphology, quality, tribological properties or mechanical properties of diamond film [11–19]. However, the influence mechanism beneath the experimental phenomenon is not clear yet. How to explain these experimental results from the point view of growth theory is of great significance to choose different dopants to get the desired diamond properties we want.

The surface chemistry of diamond films prepared by CVD is very complicated, it includes different steps such as adsorption, H abstraction and surface migration of the radicals. The growth theory of diamond films are intensively studied based on the molecular orbital theory, density functional theory (DFT), Quantum Mechanical or Monte Carlo method [20,21]. It was found that the CH_3 adsorption is one of the main growth steps of the diamond deposited, using the hot filament chemical vapor deposition (HFCVD) method under the H_2 and CH_4 atmosphere [22,23]. DFT calculation

allows the better understanding of the influence of the impurities on the growth of diamond [24–31]. However, it still need systematically comparing of the impacts of different doping on the growth of CVD diamond films.

In this study, density functional theory has been used to investigate the influence of doping sources on the growth mechanism of CVD diamond films at atomic scale. Specifically, the influence of three doping sources (B, N and Si) on the CH_3 adsorption on diamond (111) and $(100) - 2 \times 1$ surface are studied. Firstly, the CH_3 radical adsorption on the substituted atom is compared to find out whether the dopants will affect the diamond structure. The influence of doped radicals on the adsorption of CH_3 is also studied to reveal the impacts of dopants on the epitaxial growth of diamond. It provides an effective theoretical basis for the understanding of the experimental results.

2. Methodology

All theory calculations are carried out using Cambridge Sequential Total Energy Package (CASTEP) code, which is based on density functional theory [32]. The PW91 functional and spin-polarized general gradient approximation are selected under the periodic boundary conditions. The number of k points ($2 \times 2 \times 1$) was generated using the Monkhorst-Pack scheme, and the cutoff energy was set to 280 eV [18,33]. The final morphology of diamond films is determined by the growth rate of diamond (111) and (100) facets. Thus, diamond (111) and (100) models are both used to study the adsorption energy in this study. Although it is reported that the substitutional B and N dopants within the second C layer will have the largest influence on the diamond growth rate especially on the rate-determining H-abstraction step [34]. As the aim of this study is to explore whether the CH_3 radicals can still be adsorbed on the dopants, the center carbon atom in the first C layer is substituted by boron, nitrogen or silicon atoms. The calculating model shown in Figure 1 indicates a substituted boron doped diamond slab. The pink, gray and white balls are boron, carbon and hydrogen atoms, respectively. The H-terminated diamond (111) and $(100) - 2 \times 1$ slab is composed by 4- and 6-layers carbon atoms, respectively. The thickness of the vacuum is set as 10 Å to avoid the interfering between the slabs. Two layers of carbon atoms of diamond (111) and three layers of diamond $(100) - 2 \times 1$ in the bottom are fixed, while the other atoms can relax freely.
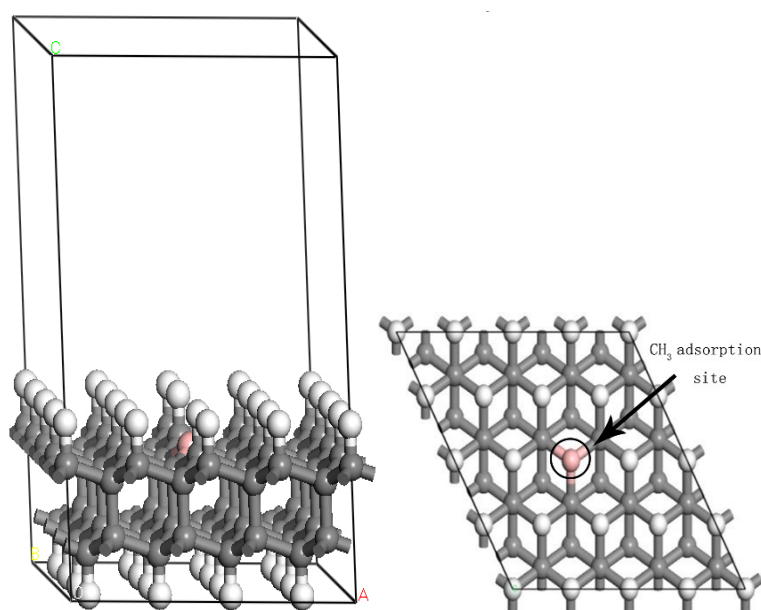

(**a**) diamond (111) surface

Figure 1. *Cont.*

(**b**) diamond (100) − 2 × 1 surface.
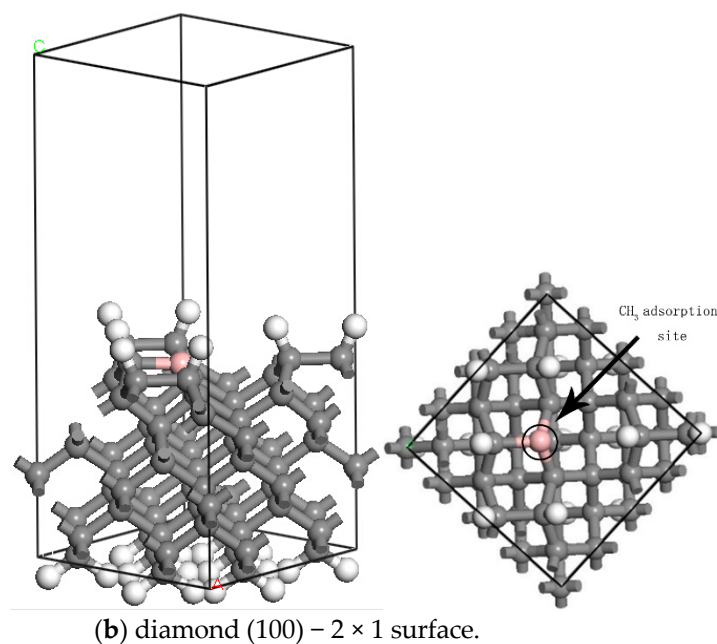
Figure 1. Representations of the supercells used in modeling the H-terminated substituted boron doped diamond surfaces.

When the effects of doped radicals on the adsorption energy of CH_3 are studied, the calculation mode is built, as shown in Figure 2. The CH_3 radical is adsorbed on the active carbon site at the center of the model, the NH_2, BH_2 or SiH_3 doped radicals are adsorbed at the C atom adjacent to the active carbon site according to the doping conditions. Due to the high symmetry of the diamond (111) surface, the carbon site adjacent the center carbon site is all equivalent. However, there are three different adsorption sites for the doped radicals on the diamond (100) − 2 × 1 reconstructed surface as shown in Figure 2b.

(**a**) diamond (111) surface.

Figure 2. *Cont.*

(**b**) diamond (100) − 2 × 1 surface.
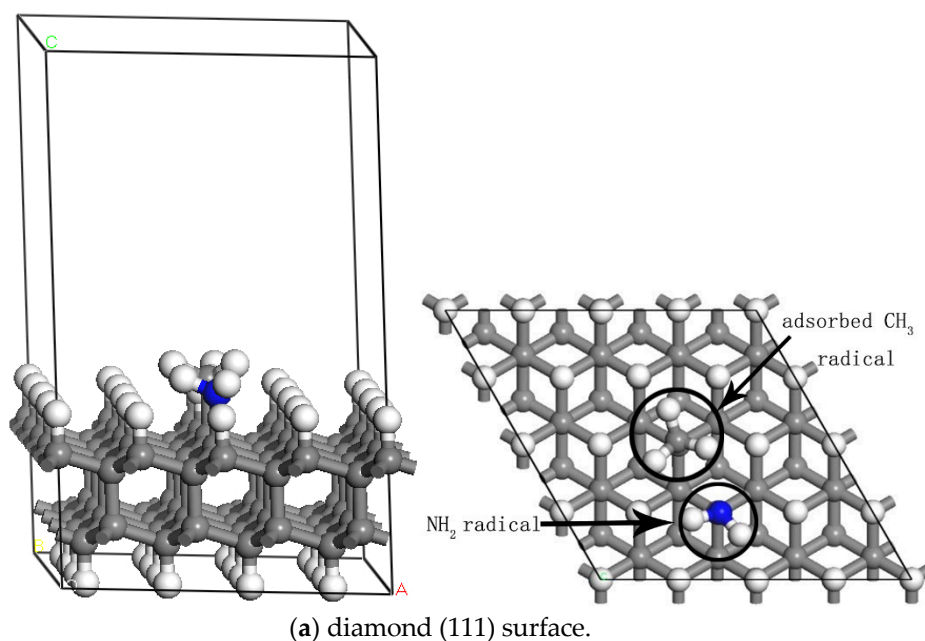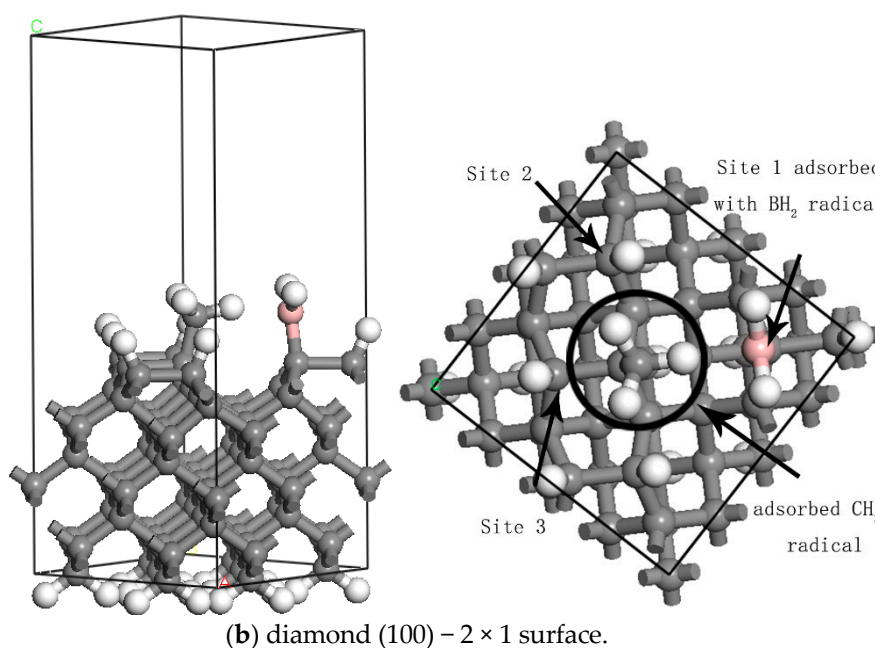
Figure 2. The calculation model which illustrate the relative position between the adsorption sites of the doped species and the radical site for CH_3 adsorption.

3. Results and Discussions

3.1. The Adsorption of CH_3 on Different Doped Atoms

The adsorption energy is defined as:

$$\Delta E_{adsorb} = E_{D\text{-}rad} - E_D - E_{rad} \tag{1}$$

Where ΔE_{adsorb} is the adsorption energy, E_D and $E_{D\text{-}rad}$ are defined as the energy before and after the adsorption of radical, respectively. E_{rad} is the energy of radical in gas phases.

The adsorption energy of CH_3 on undoped and doped (111) and (100) − 2 × 1 diamond surface is listed in Table 1. C, B, Si, N correspond to the case of undoped diamond, boron doped, silicon doped and nitrogen doped diamond, respectively. It is well known from the solid-state theory, that when the adsorption process is exoenergetic, the adsorption energy is negative and the radical can be adsorbed on the surface. Moreover, the more negative of the energy, the more stable of the adsorption. Otherwise, the radical cannot be adsorbed on the surface.

Table 1. The adsorption energy of CH_3 on undoped and substituted doped diamond surface.

ΔE_{adsorb} (kJ/mol)	(111)	(100)
C	−312.82	−349.40
B	−130.45	−234.33
Si	−360.90	−333.94
N	0.07	−37.44

Generally, the adsorption energy of CH_3 on substituted doped diamond surface is lower than that on undoped diamond surface. The adsorption energy is especially low in the case of nitrogen doped diamond. The value is almost 0 in the case of nitrogen doped diamond (111) surface. It shows that the CH_3 radical can hardly adsorbed on N atom. Moreover, the CH_3 adsorption energy is only −37.44 kJ/mol when adsorbed on the nitrogen doped diamond (100) surface. The reason for the low energy may arise from the covalent bond weakening caused by the extra electron in N. The results

reveal that N atoms disfavor the epitaxial growth of diamond on the doped site. Thus, there will be a vacancy near the N atoms and induce a larger lattice defect. Since Si has the same outer electronic structure as C, the adsorption energy of CH_3 on silicon doped diamond surface is close to that on undoped diamond surface.

Due to the adsorption energy of CH_3 on different doped diamond (100) and (111) surface sharing a same variation tendency, the cases of CH_3 adsorbed on diamond (111) surface is used for further analysis. Since the atoms in the surface region can move freely in the calculation, the change of the model geometry and the electronic structure before and after adsorption will have a significant impact on the final adsorption energy. Firstly, the charge distribution of diamond surface before CH_3 adsorption as shown in Figure 3 is analyzed. The total charge density distribution range in 0~2.35. It can be seen that the total electron density of boron doped, silicon doped and nitrogen doped diamond is similar with that of undoped one. The results indicated that the bonding structure between doped atoms and carbon atoms is similar, and there is no chemical bond breaking. It is well known that there are five valence electrons in the outer layer of N atom; pair electrons will form when the N atom interacts with three carbon atoms in the secondary layer of the diamond slab. The forming of pair electrons will enable a stable electronic structure of the diamond surface. Therefore, it can be seen from the total electron density of the diamond surface that the surrounding region of N atom is a charge enrichment region. Moreover, the charge density difference is also analyzed, and the charge density range is −0.7~0.7. The region where the electronic decreased is shown in blue, electronic enrichment is shown in red, and white indicates that electron density is almost not changed in one region. As indicated in Figure 3b, the boron atom center is blue while the nitrogen atom center is red. The results reveal that boron atom loses electrons while the nitrogen atom gets electrons. The results of Mulliken population analysis show that C has no electron gain or loss, Si lost 1.27 electrons, B loses 0.62 electrons, and N gets 0.39 electrons.
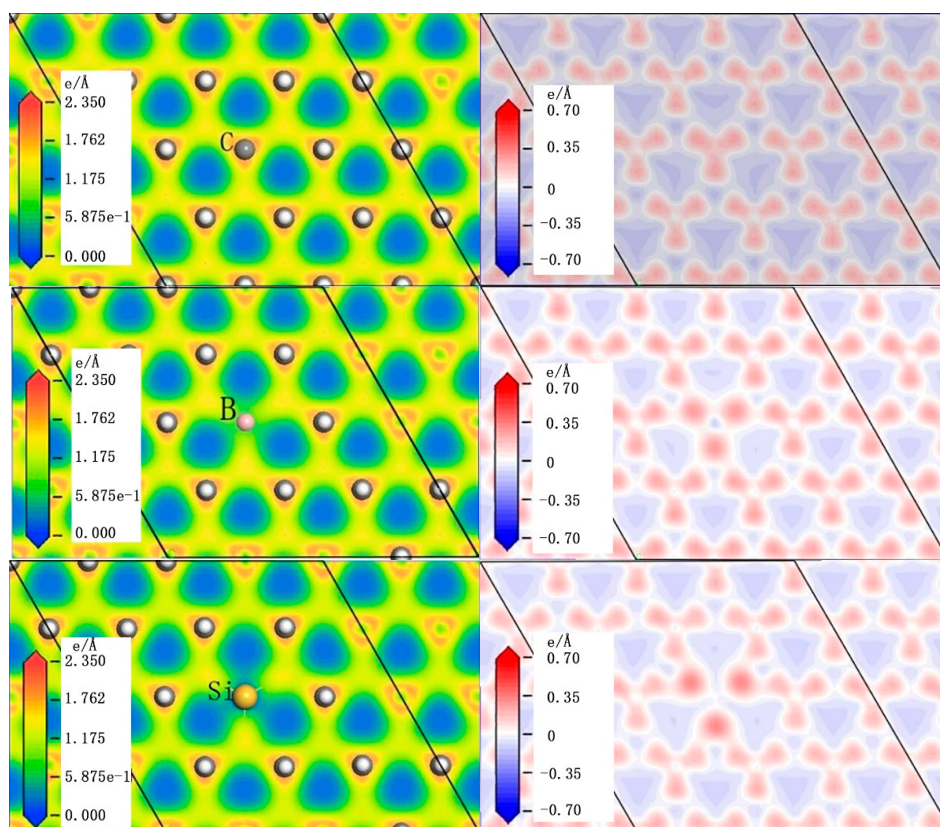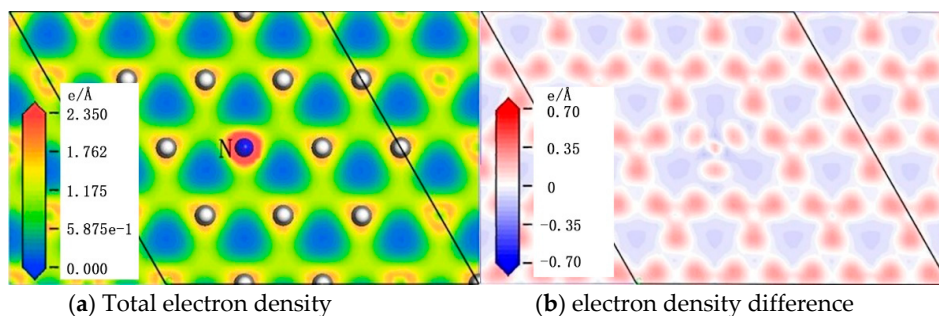

Figure 3. *Cont.*

(**a**) Total electron density   (**b**) electron density difference

Figure 3. Contours of total electron density and electron density difference on 2D slices through carbon atom and substituted B, Si and N atoms.

For all kinds of doping, the electron density difference is viewed at a selected plane with the same height. However, the bond length of Si-C is larger than that of the original C-C after silicon doping, so the plane may closer to the center of the Si-C bond compared with C-C, B-C and N-C bond. Consequently, the electron density difference shows a more pronounced electronic enrichment in the case of silicon doped diamond surface.

Figure 4 illustrates the local density of the state of the substituted atom after the adsorption of CH_3. It should be mentioned that the total energies at the zero-energy point for different models may not be identical. It can be seen that the 2s and 2p orbitals of the carbon atom have overlapped within the region of $-20{\sim}-7.5$ eV, and the overlap of 2s and 2p valence electron orbitals of B atom occurs in the energy region of $-15{\sim}-2.5$ eV. Furthermore, the overlap of 2s and 2p orbitals of silicon atom occurs in the regions of $-10{\sim}-2.5$ and $-15{\sim}-12.5$ eV. However, the overlap for the N atom within the entire energy region is very small. The results indicate that C, B, and Si atoms may bond with CH_3 due to the overlapping of the orbitals. However, N atom directly obtained three electrons provided by the C atoms bonded with the N atom located in the sublayer of the diamond bulk. As a result, the N atom comes to a full electron state before CH_3 adsorbed on the N atom. Consequently, the bonding strength between N and CH_3 is weak. The adsorption of CH_3 on the substituted nitrogen atom may be a reversible adsorption and a vacancy may easily form near the nitrogen atom.
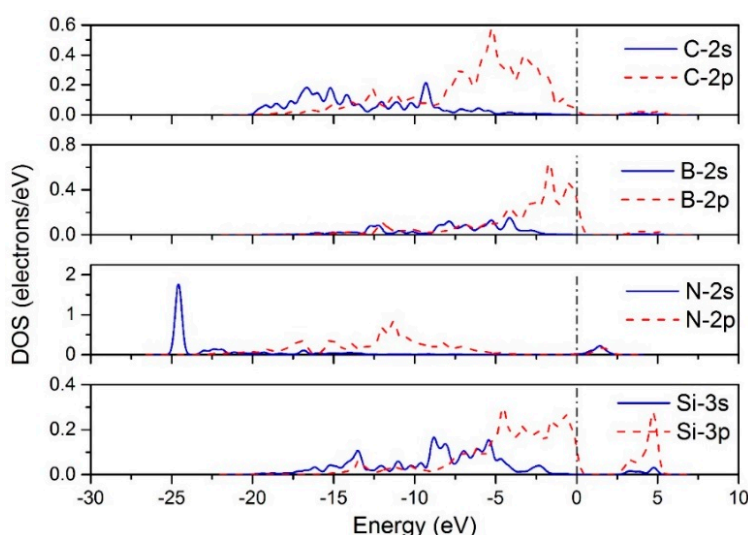

Figure 4. Local density of state of the substituted atom after the adsorption of CH_3.

The bond population between the C atom of adsorbed CH_3 and surface substitutional doped atom are calculated as follows: C-C, 0.75; C-B, 0.81; C-Si, 0.72; C-N, 0.43. The C-N bond presents a significantly lower population value compared with other types of bonds. The results indicate C-N bond is relative weaker [35]. C-Si bond shows a similar bond population value with C-C bond due

to Si and C atom having the same outer valence electron structure. It also shows that the adsorption energy of CH_3 on the Si doped diamond surface is lower than that on the undoped diamond surface. The population value of B-C is the largest, thus the B-C bond is strongest among all cases. The results indicate that the B atoms can be easily incorporated into the diamond lattice and will not have a greater impact on the further growth of the diamond.

Although the adsorption energy of CH_3 on the substituted N atom within the (100) diamond surface is lower than that of other doping cases, it still has a certain adsorption energy compared with the almost 0 in the nitrogen doped (111) diamond surface. Figure 5 shows the structure of the nitrogen doped (100) diamond before and after the adsorption of CH_3 on the substitutional nitrogen atom. It can be found that the distance between N and C3 atom increases to 2.438 Å after the CH_3 adsorption, and the N-C3 bond breaks, which indicate the occurring of the so-called beta scission rearrangement [35]. N atom only bonds with Cs1 and Cs2 atom in the secondary C layer, and N-Cs1 and N-Cs2 bond are symmetrical distributed with an equal bond length of 1.48 Å. Therefore, it has a certain adsorption energy when CH_3 adsorbed on the nitrogen doped (100) diamond surface.
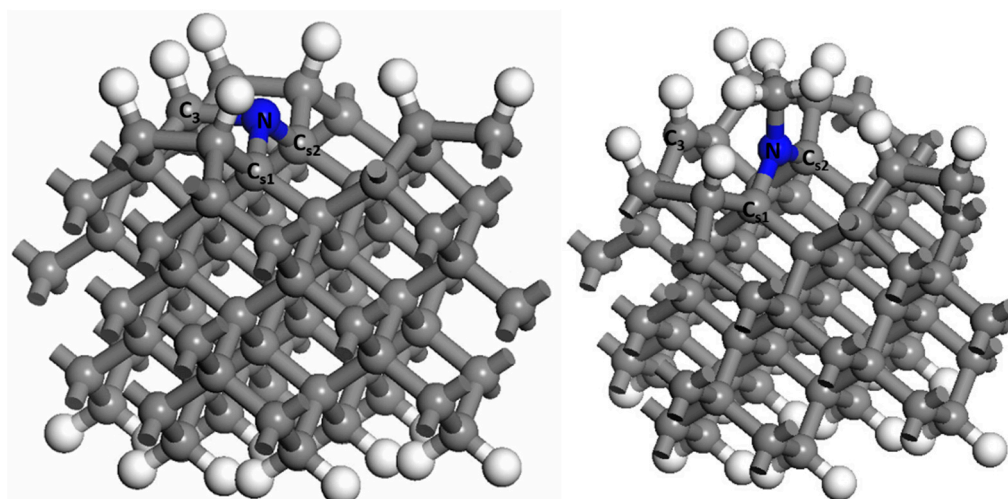
Figure 5. The model structure of N-doped diamond (100) surface before and after the CH_3 adsorption.

3.2. The Effects of Doped Radicals on the Adsorption of CH_3

The interaction between the doped radicals and CH_3 adsorbed on the surface may change the structural stability. The stable of the surface structure before the adsorption will reduce the adsorption energy, while the stable of the structure after adsorption will increase the adsorption energy. Table 2 shows the CH_3 adsorption energies in the presence of different adsorbed dopants initially adsorbed on the carbon atoms near the CH_3 adsorption site. For comparison, the adsorption energy of CH_3 is calculated under the same conditions when the adsorbed dopants are replaced by H or CH_3. The former case represents the undoped diamond growth. While the latter is mainly calculated to describe the difference of electronegativity between C, B, N, and Si, which in turn may lead to electron delocalization in the surface region of the diamond lattice. Generally speaking, doped radicals or CH_3 radicals will reduce the CH_3 adsorption energy compared with the undoped cases. It means that pre-adsorbed doped radicals may result in a transfer of this elementary reaction into a rate-limiting step, and thus hinder the epitaxial growth of diamond on (111) and (100) surface [33]. SiH_3 has a great influence on the adsorption energy of CH_3. It will reduce 35–52 kJ/mol of the CH_3 adsorption energy except in the case that SiH_3 is located at the adsorption site 1 of diamond (100) surface.

**Table 2.** CH$_3$ adsorption energies in the presence of different adsorbed dopants radicals.

ΔE_{adsorb} (kJ/mol)	(111)	(100)		
		1	2	3
BH$_2$	−320.94	−363.34	−345.23	−264.33
SiH$_3$	−271.25	−346.77	−297.71	−297.11
NH$_2$	−283.65	−319.14	−317.38	−346.77
CH$_3$	−267.87	−289.54	−299.67	−327.63
H	−314.69		−349.40	

However, the BH$_2$ radical seems have a different impact on the CH$_3$ adsorption. When BH$_2$ is adsorbed on the site 1 of diamond (100) surface, the adsorption energy slightly increases about 14 kJ/mol compared with that of undoped case. Moreover, CH$_3$ adsorption energy of CH$_3$ when BH$_2$ is adsorbed on the diamond (111) surface is higher than that on undoped diamond (111) surface. However, it is smaller than that of adsorption site 1 cases of diamond (100) surface, the adsorption energy increases about 6 kJ/mol. The result indicates that the BH$_2$ may beneficial to the CH$_3$ adsorption in these two cases. The adsorption of BH$_2$ at site 2 has a little impact on the adsorption energy which decreases only about 4 kJ/mol. Surprisingly, when BH$_2$ is at the adsorption site 3, the adsorption energy will decrease significantly, the value is as high as 85 kJ/mol.

T. Van Regemorter et al. pointed out that NH$_2$ will have steric hindrance effect with CH$_3$ [33]. Similarly, there is a strong steric hindrance between SiH$_3$ and CH$_3$. The steric hindrance will bring about the unstable surface structure after CH$_3$ adsorption, thus the adsorption energy is greatly reduced when NH$_2$ or SiH$_3$ is pre-adsorbed on diamond surface. Compared with NH$_2$ and SiH$_3$, BH$_2$ has a completely different effect on CH$_3$ adsorption. For diamond (111) and diamond (100) surface, when BH$_2$ is adsorbed on adjacent C atoms, the final structure of CH$_3$ adsorbed on diamond (111) and diamond (100) does not show obvious steric hindrance between CH$_3$ and BH$_2$. This is because BH$_2$ has an empty 2p orbit rather than non-bonding valence electron pairs existed in NH$_2$, which reduces the steric hindrance effect.

The optimization geometric structure of diamond when BH$_2$ is adsorbed on diamond (100) surface is shown in Figure 6. The results indicate that BH$_2$ will interact with active C site (C*) before the CH$_3$ adsorption when BH$_2$ is at the adsorption site 3 of diamond (100) surface. Consequently, the B atom and C* will form a new bond. The bonds between the B atom and the two adjacent carbon atoms are symmetrical and their bond length are about 1.6 Å. As a result, before the CH$_3$ adsorption, the diamond surface comes to a relatively stable energy when BH$_2$ is adsorbed at site 3. Consequently, the CH$_3$ adsorption energy will be reduced. Although there are no bonds between the B and C* atoms in the site 1 and site 2 cases, BH$_2$ radical has an approaching tendency to C*. Therefore, the adsorption energy of CH$_3$ will not be reduced when BH$_2$ is adsorbed on the site 1 and site 2. On the contrary, it may slight enhanced due to the absent of spatial exclusion between BH$_2$ and CH$_3$.

(**a**) site 1　　　　　　　　　　　(**b**) site 2　　　　　　　　　　　(**c**) site 3
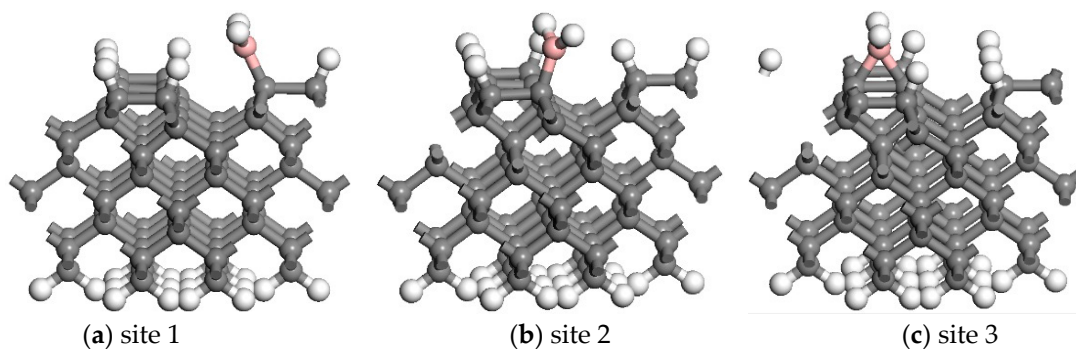
Figure 6. The optimization structure of diamond when BH$_2$ is adsorbed on diamond (100) surface before the CH$_3$ adsorption.

4. Conclusions

Hydrogen terminated diamond (111) and $(100) - 2 \times 1$ models are first used to study the adsorption possibility of CH_3 radical on substituted doped atoms. The results show that substituted silicon doping have little influence on the CH_3 adsorption due to the same outer valence electron structure between Si and C atom. The CH_3 radicals have a low adsorption energy on nitrogen doped diamond surface because of the fullness of outer electrons of nitrogen atom before the CH_3 adsorption. The adsorption of CH_3 on nitrogen doped diamond surface is only physical adsorption. While in the case of boron doped diamond, the substituted boron atom will form covalent bonds with the three-carbon atom of secondary layer of the diamond lattice. As a result, boron atoms have no redundant valence electrons, the CH_3 adsorption energy is greatly reduced. However, due to the existence of empty p orbitals of boron atoms, boron doped diamond still has a certain bonding ability. Thus, the adsorption of CH_3 on the substituted boron doped diamond surface is still chemical adsorption. Generally speaking, the adsorption energy of CH_3 on the impurity atoms is decreased, which indicates that structural defects are likely to occur near substituted doped atoms.

Subsequently, the impacts of doped radicals on the CH_3 adsorption during the initial growth of diamond films is also investigated. The results show that NH_2 or SiH_3 have a steric repulsion with CH_3, resulting in a decrease of the CH_3 adsorption energy. SiH_3 radicals will reduce the CH_3 adsorption energy by 35~52 kJ/mol. The adsorption energy of CH_3 is less affected when NH_2 is adsorbed on the adsorption site 3 (see Figure 6) of diamond $(100) - 2 \times 1$ surface. Besides that case, the presence of NH_2 on the diamond (111) and (100) surfaces will reduce the adsorption energy of CH_3 by about 30 kJ/mol. The adsorption of BH_2 radicals on the diamond $(100) - 2 \times 1$ adsorption site 3 will interact with the surface radical carbon site, resulting in a stable structure before the CH_3 adsorption. Consequently, the CH_3 adsorption energy is largely decreased by about 85 kJ/mol. However, the empty p orbital in the boron atom of BH_2 radical relieves the steric hindrance between BH_2 and CH_3 radicals. Therefore, the other BH_2 adsorption cases show little influence on the adsorption of CH_3.

The comparison of the influence of dopants on the CH_3 adsorption indicates that the Si and B atoms will not have a greater impact on the further growth of the diamond. However, the boron doping may reduce the growth rate of the diamond (100) facet at a certain CVD diamond deposition parameter. While lower the adsorption energy of CH_3 on nitrogen atom may hinder the growth of diamond near the doping point and form a vacancy diamond structure easily.

Author Contributions: Conceptualization, L.W.; Data curation, J.L.; Methodology, L.W. and J.L.; Writing—original draft, L.W.; Writing—review & editing, T.T.

Conflicts of Interest: The authors declare no conflict of interest.

References

1. Najar, K.A.; Sheikh, N.A.; Shah, M.A. Enhancement in Tribological and Mechanical Properties of Cemented Tungsten Carbide Substrates using CVD-diamond Coatings. *Tribol. Ind.* **2017**, *39*, 20–30. [CrossRef]
2. Radhika, R.; Rao, M.S.R. Growth and tribological properties of diamond films on silicon and tungsten carbide substrates. *Appl. Phys. A Mater. Sci. Process.* **2016**, *122*, 937. [CrossRef]
3. Nadolinny, V.; Komarovskikh, A.; Palyanov, Y. Incorporation of Large Impurity Atoms into the Diamond Crystal Lattice: EPR of Split-Vacancy Defects in Diamond. *Crystals* **2017**, *7*, 237. [CrossRef]
4. Ashkinazi, E.E.; Khmelnitskii, R.A.; Sedov, V.S.; Khomich, A.A.; Khomich, A.V.; Ralchenko, V.G. Morphology of Diamond Layers Grown on Different Facets of Single Crystal Diamond Substrates by a Microwave Plasma CVD in CH4-H-2-N-2 Gas Mixtures. *Crystals* **2017**, *7*, 12. [CrossRef]
5. Wang, Q.J.; Wu, G.; Liu, S.; Gan, Z.Y.; Yang, B.; Pan, J.H. Simulation-Based Development of a New Cylindrical-Cavity Microwave-Plasma Reactor for Diamond-Film Synthesis. *Crystals* **2019**, *9*, 11. [CrossRef]
6. Halliwell, S.C.; May, P.W.; Fox, N.A.; Othman, M.Z. Investigations of the co-doping of boron and lithium into CVD diamond thin films. *Diam. Relat. Mat.* **2017**, *76*, 115–122. [CrossRef]

7. Vanpoucke, D.E.P.; Nicley, S.S.; Raymakers, J.; Maes, W.; Haenen, K. Can europium atoms form luminescent centres in diamond: A combined theoretical–experimental study. *Diam. Relat. Mater.* **2019**, *94*, 233–241. [CrossRef]

8. Chou, J.P.; Retzker, A.; Gali, A. Nitrogen-Terminated Diamond (111) Surface for Room-Temperature Quantum Sensing and Simulation. *Nano Lett.* **2017**, *17*, 2294–2298. [CrossRef]

9. Bernardi, E.; Nelz, R.; Sonusen, S.; Neu, E. Nanoscale Sensing Using Point Defects in Single-Crystal Diamond: Recent Progress on Nitrogen Vacancy Center-Based Sensors. *Crystals* **2017**, *7*, 21.

10. Zou, Y.; Larsson, K. Effect of Boron Doping on the CVD Growth Rate of Diamond. *J. Phys. Chem. C* **2016**, *120*, 10658–10666. [CrossRef]

11. Srikanth, V.V.; Sampath Kumar, P.; Kumar, V.B. A Brief Review on the In Situ Synthesis of Boron-Doped Diamond Thin Films. *Int. J. Electrochem.* **2012**, *2012*, 1–7. [CrossRef]

12. Kuntumalla, M.K.; Elfimchev, S.; Chandran, M.; Hoffman, A. Raman scattering of nitrogen incorporated diamond thin films grown by hot filament chemical vapor deposition. *Thin Solid Films* **2018**, *653*, 284–292. [CrossRef]

13. Rakha, S.A.; Xintai, Z.; Zhu, D.; Guojun, Y. Effects of N_2 addition on nanocrystalline diamond films by HFCVD in Ar/CH4 gas mixture. *Curr. Appl. Phys.* **2010**, *10*, 171–175. [CrossRef]

14. Ullah, M.; Rana, A.M.; Ahmed, E.; Malik, A.S.; Shah, Z.A.; Ahmad, N.; Mehtab, U.; Raza, R. Tribological performance of polycrystalline tantalum-carbide-incorporated diamond films on silicon substrates. *Physica B* **2018**, *537*, 277–282. [CrossRef]

15. Liu, X.J.; Lu, P.F.; Wang, H.C.; Ren, Y.; Tan, X.; Sun, S.Y.; Jia, H.L. Morphology and structure of Ti-doped diamond films prepared by microwave plasma chemical vapor deposition. *Appl. Surf. Sci.* **2018**, *442*, 529–536. [CrossRef]

16. Din, S.H.; Shah, M.A.; Sheikh, N.A.; Najar, K.A.; Ramasubramanian, K.; Balaji, S.; Ramachandra Rao, M.S. Influence of boron doping on mechanical and tribological properties in multilayer CVD-diamond coating systems. *Bull. Mat. Sci.* **2016**, *39*, 1753–1761. [CrossRef]

17. Wang, L.; Liu, J.F.; Tang, T.; Xie, N.; Sun, F.H. The optimization of the doping level of boron, silicon and nitrogen doped diamond film on Co-cemented tungsten carbide inserts. *Physica B* **2018**, *550*, 280–293. [CrossRef]

18. Wang, L.; Shen, B.; Sun, F.H.; Zhang, Z.M. Effect of pressure on the growth of boron and nitrogen doped HFCVD diamond films on WC-Co substrate. *Surf. Interface Anal.* **2015**, *47*, 572–586. [CrossRef]

19. Wang, L.; Lei, X.L.; Shen, B.; Sun, F.H.; Zhang, Z.M. Tribological properties and cutting performance of boron and silicon doped diamond films on Co-cemented tungsten carbide inserts. *ScienceDirect* **2013**, *33*, 54–62. [CrossRef]

20. May, P.W.; Harvey, J.N.; Allan, N.L.; Richley, J.C.; Mankelevich, Y.A. Simulations of chemical vapor deposition diamond film growth using a kinetic Monte Carlo model. *J. Appl. Phys.* **2010**, *108*, 014905. [CrossRef]

21. Richley, J.C.; Harvey, J.N.; Ashfold, M.N.R. CH_2 group migration between H-terminated 2×1 reconstructed {100} and {111} surfaces of diamond. *J. Phys. Chem. C* **2012**, *116*, 7810–7816. [CrossRef]

22. Brenner, D.W. Empirical potential for hydrocarbons for use in simulating the chemical vapor deposition of diamond films. *Phys. Rev. B* **1990**, *42*, 9458–9471. [CrossRef] [PubMed]

23. Larsson, K.; Carlsson, J.O. Surface migration during diamond growth studied by molecular orbital calculations. *Phys. Rev. B* **1999**, *59*, 8315–8322. [CrossRef]

24. James, M.C.; Croot, A.; May, P.W.; Allan, N.L. Negative electron affinity from aluminium on the diamond (100) surface: A theoretical study. *J. Phys. Condes. Matter* **2018**, *30*, 9. [CrossRef] [PubMed]

25. Croot, A.; Othman, M.Z.; Conejeros, S.; Fox, N.A.; Allan, N.L. A theoretical study of substitutional boron-nitrogen clusters in diamond. *J. Phys. Condes. Matter* **2018**, *30*, 10. [CrossRef] [PubMed]

26. Liu, F.B.; Chen, W.B.; Cui, Y.; Jiao, Z.W.; Qu, M.; Cao, L.G. Interactions between hydrogenated diamond surface and adsorbates with different concentration of NO_2 molecules: A first-principles study. *Surf. Interface Anal.* **2018**, *50*, 962–968. [CrossRef]

27. Liu, X.J.; Qiao, H.M.; Kang, C.J.; Ren, Y.; Tan, X.; Sun, S.Y. Adsorption and migration behavior of Si atoms on the hydrogen-terminated diamond (001) surface: A first principles study. *Appl. Surf. Sci.* **2017**, *420*, 542–549. [CrossRef]

28. Tang, L.; Yue, R.F.; Wang, Y. N-type B-S co-doping and S doping in diamond from first principles. *Carbon* **2018**, *130*, 458–465. [CrossRef]

29. Cheesman, A.; Harvey, J.N.; Ashfold, M.N. Computational studies of elementary steps relating to boron doping during diamond chemical vapour deposition. *Phys. Chem. Chem. Phys.* **2005**, *7*, 1121–1126. [CrossRef]

30. Richley, J.C.; Harvey, J.N.; Ashfold, M.N.R. Boron Incorporation at a Diamond Surface: A QM/MM Study of Insertion and Migration Pathways during Chemical Vapor Deposition. *J. Phys. Chem. C* **2012**, *116*, 18300–18307. [CrossRef]

31. James, M.C.; May, P.W.; Allan, N.L. Ab initio study of negative electron affinity from light metals on the oxygen-terminated diamond (1 1 1) surface. *J. Phys. Condens. Matter* **2019**, *31*, 295002. [CrossRef] [PubMed]

32. Clark, S.J.; Segall, M.D.; Pickard, C.J.; Hasnip, P.J.; Probert, M.J.; Refson, K.; Payne, M.C. First principles methods using CASTEP. *Z. Kristallogr.* **2005**, *220*, 567–570. [CrossRef]

33. Van Regemorter, T.; Larsson, K. Effect of coadsorbed dopants on diamond initial growth processes: CH_3 adsorption. *J. Phys. Chem. A* **2008**, *112*, 5429–5435. [CrossRef] [PubMed]

34. Zhao, S.N.; Larsson, K. Theoretical Study of the Energetic Stability and Geometry of Terminated and B-Doped Diamond (111) Surfaces. *J. Phys. Chem. C* **2014**, *118*, 1944–1957. [CrossRef] [PubMed]

35. Van Regemorter, T.; Larsson, K. Effect of substitutional N on the diamond CVD growth process: A theoretical approach. *Diam. Relat. Mat.* **2008**, *17*, 1076–1079. [CrossRef]